Max–Planck–Institut für biologische Kybernetik
Max Planck Institute for Biological Cybernetics

Technical Report No. 188

Efficient Filter Flow for Space-Variant Multiframe Blind Deconvolution

Michael Hirsch[1], Suvrit Sra[1], Bernhard Schölkopf[1], Stefan Harmeling[1]

November 2009

[1] Department Schölkopf, email: hirsch;sra;bs;harmeling@tuebingen.mpg.de

This report is available in PDF–format via anonymous ftp at ftp://ftp.kyb.tuebingen.mpg.de/pub/mpi-memos/pdf/vobd_paper_mpitechreport.pdf.pdf. The complete series of Technical Reports is documented at: http://www.kyb.tuebingen.mpg.de/techreports.html

Efficient Filter Flow for Space-Variant Multiframe Blind Deconvolution

Michael Hirsch, Suvrit Sra, Bernhard Schölkopf, Stefan Harmeling
MPI for Biological Cybernetics, Spemannstrae 38, 72076 Tbingen, Germany
firstname.lastname@mpg.tuebingen.de

Abstract

Ultimately being motivated by facilitating space-variant blind deconvolution, we present a class of linear transformations, that are expressive enough for space-variant filters, but at the same time especially designed for efficient matrix-vector-multiplications. Successful results on astronomical imaging through atmospheric turbulences and on noisy magnetic resonance images of constantly moving objects demonstrate the practical significance of our approach.

1. Introduction

A wide variety of image transformations, such as convolution, blur, optical flow, illumination, non-rigid deformations, and many others, can be expressed (or sometimes at least approximated) as *linear* transformations. Restricting ourselves for notational simplicity to vector-valued images, we may write a linear image transformation as a matrix-vector-multiplication (MVM)

$$y = Ax, \tag{1}$$

where x is an input image, y is the output image, and A is the matrix expressing the linear image transformation.

Such a linear transformation matrix is considered in the Filter Flow framework of Seitz and Baker [25], who show how versatile linear transformations are. In their setup they estimate A given both x and y. Since this is a vastly underdetermined problem, they introduce a catalog of constraints to restrict the solution space. We also focus on constraining A, but with a different goal, specifically, to *efficiently* perform MVMs, because these are the essential operations for blind deconvolution algorithms.

Most prominently, if we restrict A to be a convolution matrix, then the MVM Ax is equal to the space-invariant convolution $a * x$ for an associated point-spread function (PSF) a. In this case, the MVMs for A and A^T can be calculated rapidly using Fast Fourier Transforms (FFTs). Since $a * x$ is also linear in a, there exists furthermore a matrix X such that $a * x = Ax = Xa$. Even for X and X^T the corresponding MVMs can be performed efficiently. All these four MVMs are particularly important for the problem of blind deconvolution (BD) where both the PSF a, parameterizing the matrix A, and the true image x are unknown. Only given the blurry image y, the task is to recover the true underlying image x and possibly the PSF as well. A common approach to this problem is an alternating least-squares method which *does* require all four MVMs mentioned above.

Understandably, space-invariant convolutions are severely restrictive compared with general linear transformations, which are usually computationally prohibitive [25]. Hence it is of great practical value to introduce a class of space-variant linear transformations for which the MVMs wrt both x and the parameters a (of the linear transformation A) can be calculated efficiently.

Main contribution: This paper introduces and details a framework for "Efficient Filter Flow" (EFF) that allows rapid MVMs for A, A^T, X, and X^T while simultaneously being expressive enough to provide space-variant filtering. Our framework enables us to tackle space-variant blind deconvolution for multiple frames, and we demonstrate our setup on two real-world scientific applications.

2. Related Work

Deconvolution. Removing the effects of blurring by deconvolution is a well-studied problem. In its simplest setup, the blur is assumed to be global and known, and one can apply methods such as the Richardson-Lucy algorithm [24, 21] to deconvolve the image. Even in this simple case, the ill-posedness of the deconvolution problem makes it impossible to obtain perfect solutions [12]; the difficulties are further compounded by noise. The next step is to consider blurs that are spatially-variant (though often a local-invariance is assumed). Early relevant work includes [20], where the authors cleanly formalize space-variant imaging systems, and discuss basic special cases such as: piecewise space-invariant systems and geometric distortion.

Blind-Deconvolution. More relevant to our paper is work on blind-deconvolution. Here the blur kernel is unknown, which dramatically complicates the deconvolution problem; we refer the reader to [17] for a survey. An overview and evaluation of recently proposed and state-of-the-art decon-

volution algorithms is in [19], where Levin *et al*. also ascertained that the space-invariance assumption is frequently violated in practice. We focus on space-variant blind-deconvolution, with emphasis on efficient computation.

Bascle *et al*. [4] used multiple blurred frames to generate a single deblurred image; Yuan *et al*. [31] used a pair of blurred and noisy images, though with space-invariant kernels. Rav-Acha and Peleg [23] treat images blurred in different directions to obtain a better estimate of the blur; Cho*et al*. [7] use multiple blurry images (usually two), using segmentation to isolate parts with invariant blurs. Bardsley *et al*. [3] use phase-diversity combined with the non-blind procedure of [22] to perform space-variant blind-deconvolution. Levin [18] segmented the image into multiple layers, assuming an invariant kernel for each layer; Fergus *et al*. [9] use natural image statistics to guide the blur estimation; Dai and Wu [8] present a method based on alpha-matting and segmentation to recover the blur kernel; Agrawal and Xu [1] use coded-apertures in conjunction with the motion-from-blur method of [8]; Shan *et al*. [26] use only a single image, but admit only rotational blurs; Tai *et al*. [29] use a hybrid camera setup inspired by [5].

Efficient Computation: An idea key to our framework was introduced by Stockham [28], who presented the overlap-add (OLA) method for fast convolution and correlation. For 1D signals, such as audio, Allen [2] used OLA, aka short-time Fourier analysis and synthesis for time-variant filtering. However, he considered Ax only and did not show how to calculate $A^\mathsf{T}x$, which is required for deconvolution. Neither does he show how to calculate $X^\mathsf{T}y$, which is required for blind-deconvolution. For two dimensional signals, Hinman [14] generalized short-time Fourier analysis to short-space Fourier analysis, but did not consider synthesis needed for space-variant filtering. Nagy [22] does consider synthesis, but only for rectangular and triangular windows; he also considers A and A^T only, thus non-blind.

3. Efficient Filter Flow

For simplicity we introduce our framework for vector-valued images. The generalization to matrix-valued images is straightforward. We quickly review space-invariant filters; this sets the notation and lays the foundation for our framework for space-variant filters.

3.1. Space-invariant linear filters

A particularly useful subset of the linear transformations are space-invariant filters. These filters can be represented by a vector a (of some length k), and their operation can be defined as a convolution of x with a,

$$y_i = \sum_{j=0}^{k-1} a_j x_{i-j} \quad \text{for } 0 \le i < m. \tag{2}$$

The filter a is also called the point-spread function (PSF). Recall that x is of length n and y of length m. We choose to chop the valid part from the full convolution so that $m = n - k + 1$. Since the transformation (2) is linear in x and can be written as $y = Ax$ for $A_{i,i+j} = a_j$ for $0 \le i < m$ and $0 \le j < k$. In other words A contains in each row a shifted copy of a. For such a structured A, MVMs can be performed in $O(n \log n)$ multiplications using FFTs with appropriate zero-padding. If the signal is much longer than the PSF, *i.e*., $n \gg k$, then the MVMs can be processed even faster by chunking the signal into patches and using the overlap-add (OLA) method of Stockham [28]. If q is the size of the FFT for the patches, then OLA costs $O(n \log q)$. We explain OLA in greater detail below as it forms the basis of our framework for efficient space-variant linear filters.

3.2. Efficient space-variant linear filters

A full-blown space-variant filter is computationally infeasible, while for many real-world applications space-invariant convolutions are too restrictive. Therefore, it is natural to seek a compromise. Our compromise is to define space-variant linear filters that can be computed almost as efficiently as space-invariant linear filters. The key idea behind this efficiency is to modify the overlap-add (OLA) method to calculate space-variant linear filters.

The usual OLA method chops the image into overlapping patches, damps the borders of each patch with some windowing function, convolves each patch with the same filter, and then adds the transformed patches to obtain the output image. If each patch is processed with its own filter we get a space-variant linear filter.

Formally, suppose we use p overlapping patches of an input image x. For patch r ($0 \le r < p$) we use the windowing function $w^{(r)}$ (represented as a vector of the same length as x) that is non-zero only for the interval of the corresponding patch in x. Entry-wise multiplication of $w^{(r)}$ with x, sets all entries in x outside the r-th patch to zero, windowing the remaining entries. Denoting the p filters of length k by $a^{(r)}$ ($0 \le r < p$), our space-variant OLA (SVOLA) filtering is

$$y_i = \sum_{r=0}^{p-1} \sum_{j=0}^{k-1} a_j^{(r)} w_{i-j}^{(r)} x_{i-j} \text{ for } 0 \le i < m. \tag{3}$$

For fixed patch size and fixed number of patches, the amount of overlap and the locations of the patches can be easily calculated. The parameters of the SVOLA filtering are the k PSFs $a^{(0)}, \ldots, a^{(k-1)}$.

3.2.1 Allowable window functions

Care must be taken when choosing window functions since they must add up to one, that is,

$$\sum_{r=0}^{p-1} w_i^{(r)} = 1 \quad \text{for } 0 \le i < m. \tag{4}$$

Without this property artefacts will show up in the output image y at the overlapping areas of the patches. In practice, this property can always be enforced by normalizing the window functions.

3.3. Efficient MVMs for SVOLA

Now that we have defined the space-variant version of OLA, we come to the most important part: efficient implementation of the MVMs.

Since x appears only linearly in Eq. (3), we can write it as $y = Ax$. The filter matrix A is given by

$$A = \sum_{r=0}^{p-1} \operatorname{Diag}\big(w^{(r)}\big) A^{(r)}, \tag{5}$$

where $A^{(r)}$ is the matrix corresponding to the convolution $a^{(r)}$ $(0 \le r < p)$, and $\operatorname{Diag}(v)$ is a diagonal matrix that has vector v along its diagonal. However, this representation does not describe how MVMs with A, nor with A^T, can be efficiently computed. For that we equivalently express A as the following sum of a product of matrices

$$y = \underbrace{Z_y^\mathsf{T} \sum_{r=0}^{p-1} C_r^\mathsf{T} F^\mathsf{H} \operatorname{Diag}(F Z_a a^{(r)}) F C_r \operatorname{Diag}(w^{(r)})}_{A} x. \tag{6}$$

Equation (6) looks complicated, but is simple to understand. Here are the details: (i) C_r is a matrix that chops the r-th patch from a vector of length n; (ii) Z_a is a zero-padding matrix that appends zeros to $a^{(r)}$ such that its size matches the patch size; (iii) F is the Discrete Fourier Transform (DFT) matrix (implemented by FFT); (iv) F^H is the Hermitian of the the DFT matrix (implemented by inverse FFT); and (v) Z_y is the zero-padding matrix that prepends zeros to a vector such that its size matches the size of the vector resulting from the summation.

The proof that A in Eq. (5) is the same as in Eq. (6) follows directly from the FFT implementation of convolution. Reading (6) from right to left this expression succinctly describes the steps needed to efficiently compute Ax. We can also read off A^T as

$$A^\mathsf{T} = \sum_{r=0}^{p-1} \operatorname{Diag}(w^{(r)}) C_r^\mathsf{T} F^\mathsf{T} \operatorname{Diag}(F Z_a a^{(r)}) \overline{F} C_r Z_y \tag{7}$$

$$= \sum_{r=0}^{p-1} \operatorname{Diag}(w^{(r)}) C_r^\mathsf{T} F^\mathsf{H} \overline{\operatorname{Diag}(F Z_a a^{(r)})} F C_r Z_y, \tag{8}$$

where $\overline{A}$ is the component-wise complex conjugate of A. Eqn. (8) follows from (7) because A is a real valued matrix, whereby $A = \overline{A}$. Reading (8) from right to left describes the steps needed to efficiently calculate MVM for A^T. In words, we perform steps similar to SVOLA on y but with windowing at the end instead of the beginning, and with complex conjugation of the FFT of the PSFs, resulting in calculating patch-wise correlations instead of convolutions.

For non-blind deconvolution case with a space-variant filter A, efficient MVMs with A and A^T suffice. But for blind deconvolution we need more. Since Eq. (3) is also linear in the k PSFs, we next define a matrix X such that $y = Ax = Xa$, where a denotes the stacked sequence of PSFs $a^{(0)}, \ldots, a^{(p-1)}$. Now we rewrite (6) using $D(v)w = D(w)v$ and some matrix B_r that chops the r-th PSF from the vector a,

$$y = \underbrace{Z_y^\mathsf{T} \sum_{r=0}^{p-1} C_r^\mathsf{T} F^\mathsf{H} \operatorname{Diag}\big(F C_r \operatorname{Diag}(w^{(r)}) x\big) F Z_a B_r}_{X} a. \tag{9}$$

This expression is not needed for implementing Xa since we already know how to compute $Ax = Xa$ quickly, but it allows us to derive an algorithm for efficient MVM with X^T simply by taking the transpose of the expression for X,

$$X^\mathsf{T} = \sum_{r=0}^{p-1} B_r^\mathsf{T} Z_a^\mathsf{T} F^\mathsf{T} \operatorname{Diag}\big(F C_r \operatorname{Diag}(w^{(r)}) x\big) \overline{F} C_r Z_y, \tag{10}$$

$$= \sum_{r=0}^{p-1} B_r^\mathsf{T} Z_a^\mathsf{T} F^\mathsf{H} \overline{\operatorname{Diag}\big(F C_r \operatorname{Diag}(w^{(r)}) x\big)} F C_r Z_y, \tag{11}$$

where we again used $X = \overline{X}$, as X is real. In words, the algorithm implied by (11) for $X^\mathsf{T} v$ consists of splitting v into patches, correlating them with the patches from x, and finally summing up the results.

3.4. Computational complexity

The computational complexity of SVOLA-based MVMs for A, A^T, X, and X^T is the same as the OLA method for space-invariant filtering which is about $O(n \log q)$, where q is the size of the FFT for the patches. Thus we see that the SVOLA is as efficient as the space-invariant filtering. Since the PSFs $a^{(r)}$ are much smaller than the input image x, the memory requirement for storing the space-variant filter is much less than $O(mn)$ needed by a general linear transformation. We note, however, that estimating the parameters for SVOLA-based transformations (e.g., in blind deconvolution), is usually more costly, since the number of parameters increases with the number of patches, while for space-invariant filters, only a single filter needs to estimated.

3.5. Expressivity

Obviously, a space-invariant filter represented by a PSF a is a special case of the SVOLA filtering. When all PSFs $a^{(r)} = a$, using (4), we see that (3) reduces to (2).

At the other extreme, SVOLA filtering can implement *any* linear transformation A. To do so, we need m image patches, one for each row of A. Then, we set all window functions to constant $1/m$, and the PSFs characterizing the SVOLA filtering to the rows of A. This case is degenerate as patches overlap completely and PSFs, as long as the signal, are only evaluated once. But it shows that SVOLA filtering actually covers the entire range from to space-invariant filtering to arbitrary linear transformations, trading computational efficiency for being more expressive.

Figure 1 shows further examples what kind of image transformations our framework is able to express.

4. Space-Variant Blind Deconvolution

Least-squares based alternating minimization methods offer a simple but effective choice for blind-deconvolution. Here one estimates the image x given A and y by minimizing $\|Ax - y\|^2$; analogously one estimates a given x and y by minimizing $\|Xa - y\|^2$ (a and X were introduced in Sec. 3.3). It is also natural to add non-negativity constraints on x and a, so that both minimizations are essentially special cases of the non-negative least-squares problem, $z = \operatorname{argmin}_{z \geq 0} \|Bz - y\|^2$, which is commonly solved using: (i) constrained optimization using its gradient $2B^\mathsf{T}(Bz - y)$ wrt. z; and (ii) using multiplicative updates,

$$z \leftarrow z \odot \frac{B^\mathsf{T} y}{B^\mathsf{T} B z} \tag{12}$$

where the Hadamard product $\odot$, and the fraction bar denote component-wise multiplication and division, respectively.

Both gradient-based and multiplicative methods were used by Harmeling *et al*. [13] for deriving an efficient online algorithm for multiframe blind deconvolution. Their algorithm recovers a true image x given a sequence of noisy and blurred images $y^{(0)}, \ldots, y^{(s-1)}$, each of which is modeled as $y^{(t)} = A^{(t)}\, x + n^{(t)}$, for $0 \leq t < s$. The noise $n^{(t)}$ is assumed to be zero-mean Gaussian, and the transformation matrices $A^{(t)}$ are unknown.

Harmeling *et al*. showed the effectiveness of processing the image sequence $y^{(0)}, \ldots, y^{(s-1)}$ using the following two steps in alternatingly:

1. Given x and $y^{(r)}$ estimate the PSF $a^{(r)}$, parameterizing $A^{(r)}$, using constrained optimization,

2. Given $A^{(r)}$ and y update the true underlying image x by a single multiplicative update step, as in (12).

At the beginning x is initialized by the first observation $y^{(0)}$.

However, Harmeling *et al*. [13] considered only space-invariant convolutions. Thus the immediate question is whether their online algorithm for multiframe blind deconvolution can be combined with our framework of space-variant filtering? The answer is 'yes' and will be proven in the following experimental section.

5. Experiments

Our work is motivated by two main application areas: (i) ground-based astronomical observations through turbulences of the atmosphere, and (ii) magnetic resonance imaging (MRI) of objects in constant motion with high noise. In the following we present results for both problems that demonstrate that our framework for efficient filter flow does solve these real-world problems. However, for both applications there is no ground truth available, so additionally we show controlled lab experiments with known ground truth which we describe first.

5.1. Controlled lab experiments

To verify and evaluate our approach we recorded several image sequences under controlled conditions. For these experiments we mounted a Canon EOS 5D Mark II camera equipped with a 200 mm zoom lens on a tripod on a platform roof and captured a static scene through hot air exhausted by the building's vent, which could be closed to take sharp images of the same scene. The sequences consist of 100 frames degraded by spatially-varying blur (each with an exposure time of 1/250s). Figure 4 shows typical frames and in the last row the reconstructed images. The images of the "chimney" and the "building" sequences have size 237×237 pixels, the images of the "books" sequence have size 109×109 pixels. For all three sequences we choose a Bartlett-Hanning window with 50%overlap. We modelled the space-variant blurs with 3×3 PSFs. Figure 3 compares our reconstructed images (left column) with the sharp ground-truth images. For all three image sequences the reconstructed images reveal great faithfulness in detail and high-frequency structure confirming both our image model and the presented blind deconvolution algorithm.

5.2. Looking through atmospheric turbulences

The top row of Figure 2 shows typical frames from an image sequence of the central massive of the lunar crater Copernicus. The original recording was taken with a 14-inch f/10 Celestron C14 and a DMK 31 AF03 CCD camera from Imaging Source at a frame rate of 30 fps with an exposure time of 10 ms. The field of view is 227x227 pixels in size, which corresponds to an angular size of approximately 16", which is despite the good seeing conditions at the time of recording, beyond the isoplanatic patch. Thus space-variant filters are needed to describe the image deforma-

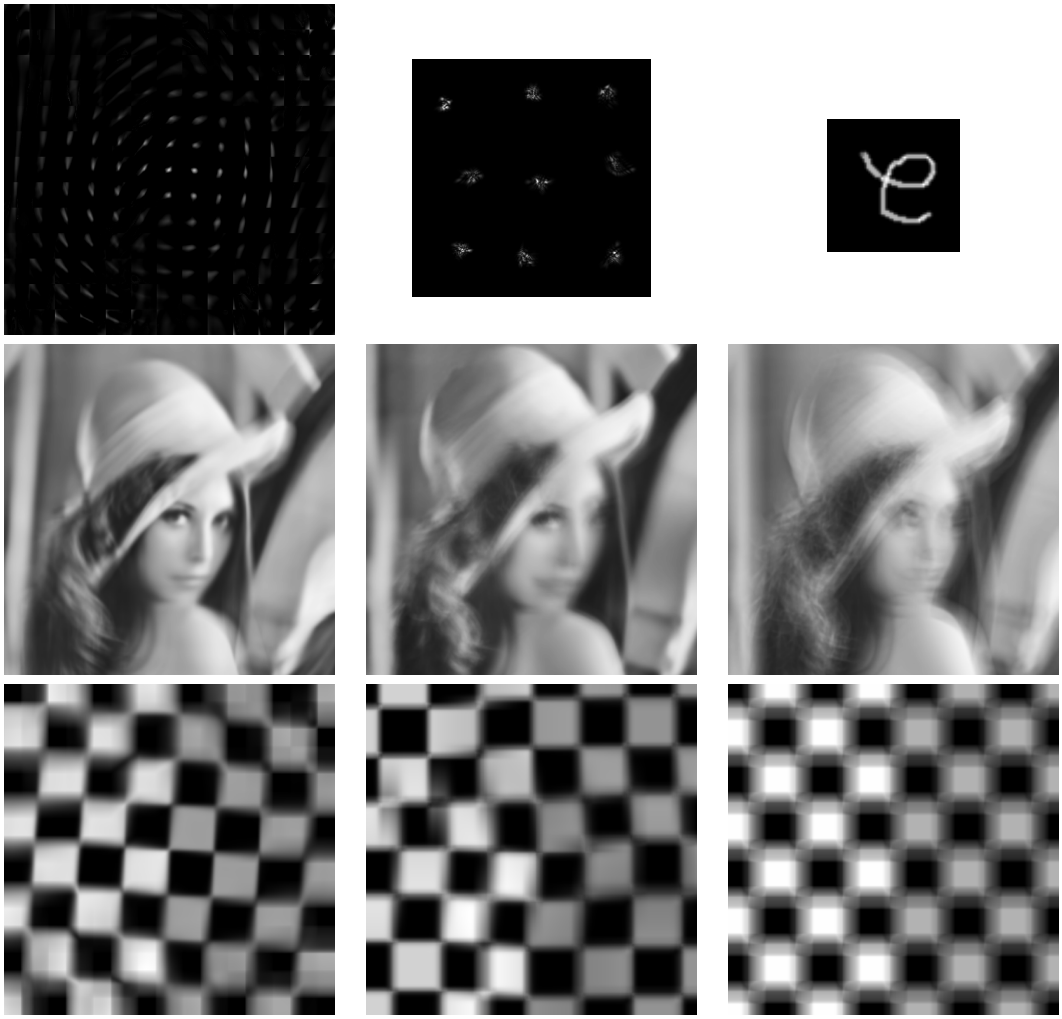

Figure 1. Expressivity of our proposed SVOLA framework; (left to right) Rotational transformation approximated by a spatially-varying PSF with 13x13 kernels each 41x41 pixels in size, atmospheric blur with 3x3 different speckle patterns each, global motion blur, expressable by one single PSF.

tion caused by the atmosphere. The bottom row of Figure 2 shows the results of state-of-the-art reconstruction methods after having processed 200 frames. From left to right we show the subjectively best observed frame, a reconstruction with AviStack, a standard "lucky imaging" software [10, 30], a Knox-Thompson reconstruction [16, 27] (using 300 Know-Thompson and 100 triple correlation phase pairs), the results of Harmeling *et al*. [13] (with PSF size 31×31 pixels and Tikhonov regularization for the PSF), and of BD based on EFF. We modelled the recorded frames as an EFF with 3×3 PSFs of size 31×31 pixels and a Bartlett-Hanning window of size 128×128 with 50% overlap to model the space-variant blur. For none of the method further post-processing was performed.

Not surprisingly, the reconstruction with AviStack is only slightly better than the visually best observed frame. By comparison, the result of the Knox-Thompson method reveals greater detail and higher spatial resolution. Despite the violated assumption of isoplanacity, the reconstucted image modelled by a single PSF is comparable in quality to the Knox-Thompson reconstruction. Compared to the previous images, our estimated image under the assumption of a spatially varying PSF shows even more detail and reveals structure unresolved in the previous images.

5.3. MRI of objects in motion

The second application addresses the common problem of object motion in Magnetic Resonance Imaging (MRI). MRI is a medical imaging modality for visualising the internal structure and function of the human body and animals used in preclinical studies. Compared to computed tomography (CT), MRI provides much greater contrast between different soft tissues, that makes it especially useful in neurological (brain), musculoskeletal, cardiovascular, and on-

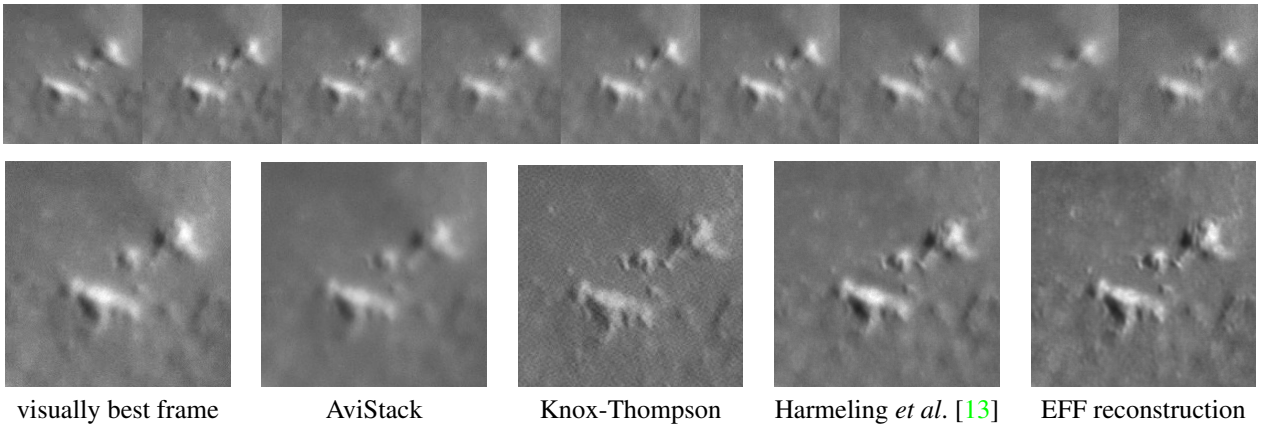

Figure 2. Copernicus Crater: top row shows typical observed frames; bottom row compares our approach against other state-of-the-art methods.

Figure 3. Results from the EFF reconstruction compared to ground truth for the controlled experiments.

cological (cancer) imaging.

Figure 6 shows typical frames of two image sequences of a mouse's thorax in a preclinical study for contrast MRI. The sequences correspond to two axial slices at different height. Both were taken with a 7 Tesla ClinScan of Bruker and consist of 200 frames, each 128×128 pixel in size. As can be seen from these frames, object motion produces large blurs and leads to a significant loss in image quality. Besides global object motion also the heart beat causes local distortions. Both global and local deformations can be described by our framework for space-variant filtering. Thus we applied our space-variant blind deconvolution algorithm with 4×4 PSFs of size 20×20 pixels (choosing a Bartlett-Hanning window of size 64×64 pixels with 50% overlap). For kernel estimation we imposed additional Tikhonov regularization. Figure 6 shows the estimated images of our method. More interestingly, our method can be used for effective motion correction, as at each time step the estimated object image remains at the same position. Dropping the energy constraint on the kernel, the estimated PSFs give not only information about the object motion, but also about the intensity change, which is of mayor interest in contrast or functional MRI. For comparison Figure 5 compares our results with a state-of-the-art method for non-rigid registration from Friston *et al*. [11]. We clearly see that our method recovers more image details.

6. Discussion and Conclusion

We introduced a powerful framework for space-variant blind-deconvolution by considering a structurally restricted set of admissible linear filters. Our framework offers an efficient compromise between the extremes of space-invariance and full-dense linear transformations. We extended the overlap-add idea to the space-variant setting, thereby allowing us to compute matrix-vector-multiplications involving the filter rapidly using FFTs. We applied our framework to real-world blind-deconvolution applications drawn from astronomy and medical imaging. We obtained very encouraging results, using an efficient online algorithm, without taking resort to expensive equipment like hybrid cameras.

Some questions do remain open at this point. The first one is how to further improve the runtime of kernel estimation, especially because the number of parameters involved

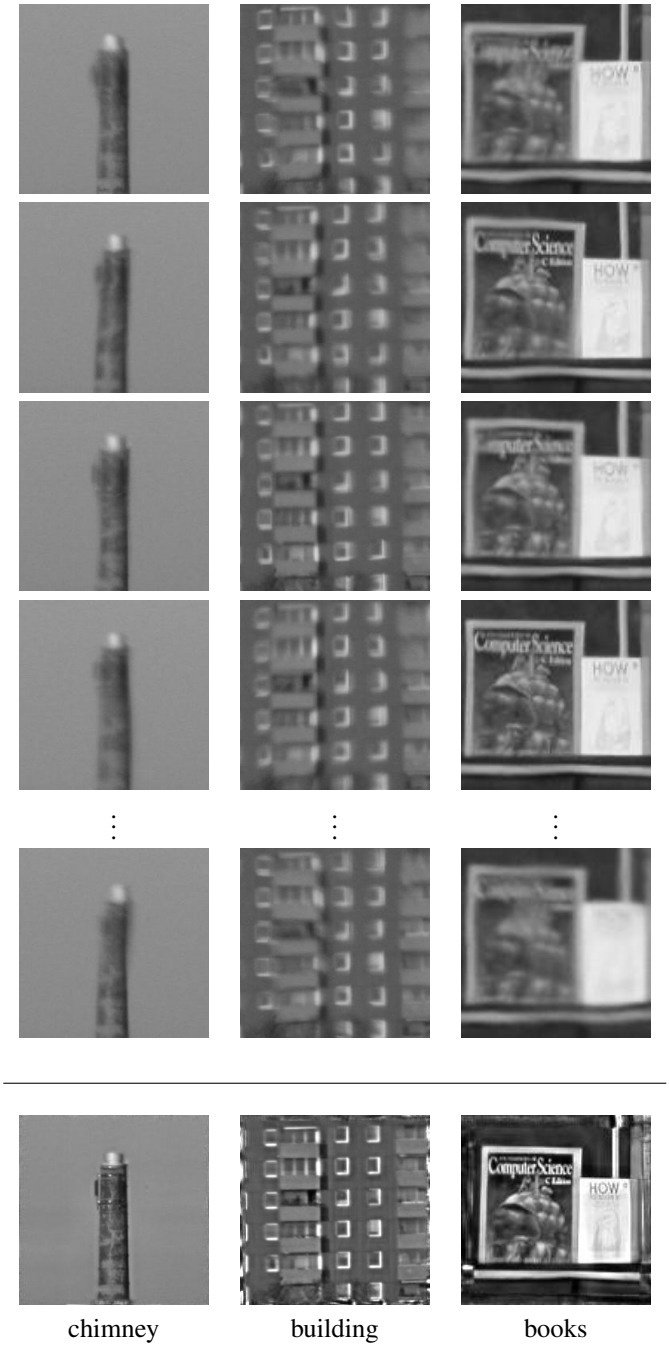

chimney building books

Figure 4. EFF reconstruction (bottom row) and typical frames from the controlled experiments.

can be large. For kernels (per patch) of sizes 31×31 the runtime lies in minutes, though for sizes of 15×15 the runtime is in seconds. For speeding up kernel estimation, we did try the recent ideas of Joshi *et al*. [15] and Cho *et al*. [6]. But in our experiments, the presence of noise led to unfavorable kernel estimates. Another method of speedup could be by using GPUs for computation, though the large amount of data transfer could impede an easy speedup.

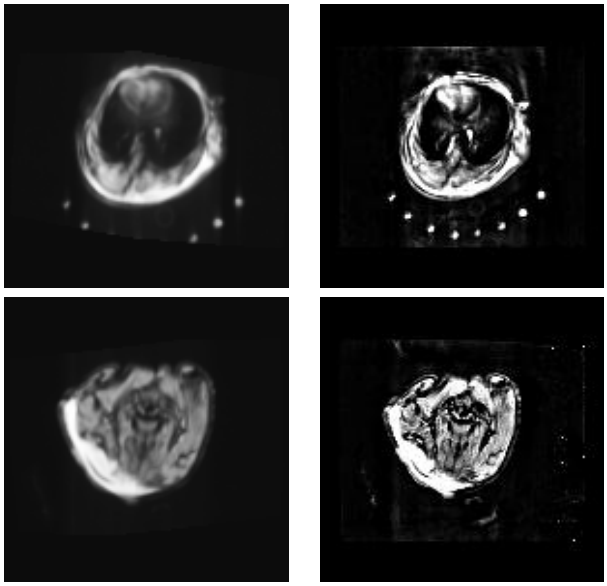

Friston *et al*. [11] EFF reconstruction

Figure 5. MRI of objects in motion: comparison to the non-rigid registration method of Friston *et al*. [11] versus our approach

Other immediate open questions that we wish to investigate in the future include application of our framework to other domains where space-variant blind-deconvolution is important, e.g., to electron microscopy.

References

[1] A. Agrawal and Y. Xu. Coded Aperture Deblurring: Optimized Codes for PSF Estimation and Invertibility. In *CVPR*, 2009. 2

[2] J. Allen. Short term spectral analysis, synthesis, and modification by discrete Fourier transform. *IEEE Transactions on Acoustics, Speech and Signal Processing*, 25(3):235–238, 1977. 2

[3] J. Bardsley, S. Jeffries, J. Nagy, and B. Plemmons. A computational method for the restoration of images with an unknown, spatially-varying blur. *Optics Express*, 14(5):1767–1782, 2006. 2

[4] B. Bascle, A. Blake, and A. Zisserman. Motion deblurring and super-resolution from an image sequence. In *ECCV*, 1996. 2

[5] M. Ben-Ezra and S. K. Nayar. Motion deblurring using hybrid imaging. 2003. 2

[6] S. Cho and S. Lee. Fast motion deblurring. *ACM Transactions on Graphics (SIGGRAPH ASIA 2009)*, 28(5):article no. 145, 2009. to appear. 7

[7] S. Cho, Y. Matsushita, and S. Lee. Removing non-uniform motion blur from images. *Computer Vision, 2007. ICCV 2007. IEEE 11th International Conference on*, pages 1–8, Oct. 2007. 2

[8] S. Dai and Y. Wu. Motion from blur. In *IEEE CVPR*, pages 1–8, 2008. 2

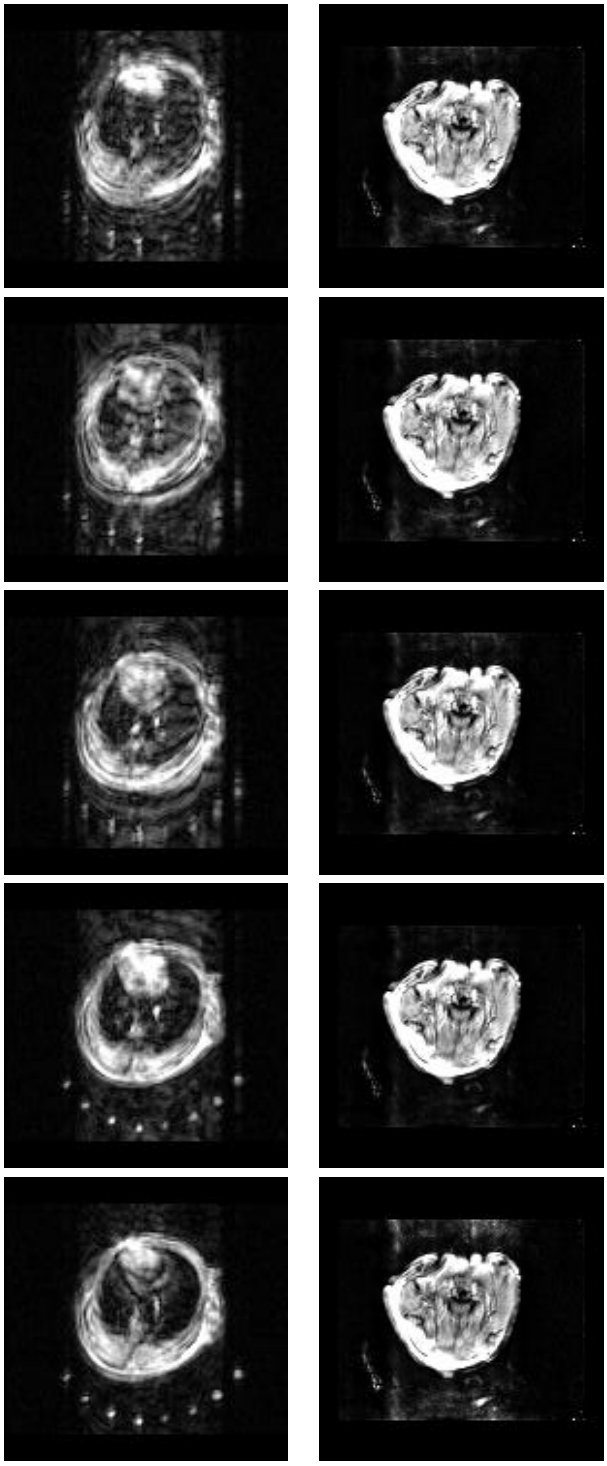

Figure 6. Typical frames of axial slices of a mouse thorax.

[9] R. Fergus, B. Singh, A. Hertzmann, S. T. Roweis, and W. T. Freeman. Removing camera shake from a single image. *ACM Transactions on Graphics (SIGGRAPH)*, 2006. 2

[10] D. L. Fried. Probability of getting a lucky short-exposure image through turbulence. *J. Optical Soc. Amer.*, 86(1651-1657), 1978. 5

[11] K. Friston, J. Ashburner, C. Frith, J. Poline, J. Heather, and R. Frackowiak. Spatial registration and normalization of images. *Human Brain Mapping*, 2(1):1–25, 1995. 6, 7

[12] D. Geman and G. Reynolds. Constrained Restoration and the Recovery of Discontinuities. *IEEE Trans. Pattern Anal. Mach. Intell.*, 14(3):367–383, 1992. 1

[13] S. Harmeling, M. Hirsch, S. Sra, and B. Schölkopf. Online blind image deconvolution for astronomy. In *Proceedings of the IEEE Conference on Comp. Photogr.*, 2009. 4, 5, 6

[14] B. Hinman, J. Bernstein, and D. Staelin. Short-space Fourier transform image processing. *IEEE International Conference on ICASSP*, 9:166–169, Mar. 1984. 2

[15] N. Joshi, R. Szeliski, and D. J. Kriegman. Image/video deblurring using a hybrid camera. In *CVPR*, 2008. 7

[16] K. T. Knox and B. J. Thompson. Recovery of images from atmospherically degraded short-exposure photographs. *Astrophysical J.*, 193:L45–L48, 1974. 5

[17] D. Kundur and D. Hatzinakos. Blind image deconvolution. *IEEE Signal Processing Mag.*, 13(3):43–64, May 1996. 1

[18] A. Levin. Blind motion deblurring using image statistics. In *Advances in Neural Information Processing Systems (NIPS)*, 2006. 2

[19] A. Levin, Y. Weiss, F. Durand, and W. T. Freeman. Understanding and evaluating blind deconvolution algorithms. In *CVPR*, 2009. 2

[20] A. W. Lohmann and D. P. Paris. Space-Variant Image Formation. *J. Opt. Soc. Amer.*, 55(8), Aug. 1965. 1

[21] L. Lucy. An iterative technique for the rectification of observed distributions. *J. Astronomy*, 79:745–754, 1974. 1

[22] J. G. Nagy and D. P. O'Leary. Restoring images degraded by spatially variant blur. *SIAM Journal on Scientific Computing*, 19(4):1063–1082, 1998. 2

[23] A. Rav-Acha and S. Peleg. Two motion-blurred images are better than one. *Pattern Recogn. Lett.*, 26(3):311–317, 2005. 2

[24] W. Richardson. Bayesian-based iterative method of image restoration. *J. Opt. Soc. of Am.*, 62(1), 1972. 1

[25] S. Seitz and S. Baker. Filter Flow. In *Proc. Int. Conf. on Computer Vision*, 2009. 1

[26] Q. Shan, W. Xiong, and J. Jia. Rotational motion deblurring of a rigid object from a single image. In *Proc. Int. Conf. on Computer Vision*, 2007. 2

[27] C. Stelzer and H. Ruder. Suppressing anisoplanatism effects in speckle interferometry. *Astronomy and Astrophysics*, 475(2):771–774, 2007. 5

[28] T. Stockham Jr. High-speed convolution and correlation. In *Proceedings of the April 26-28, 1966, Spring joint computer conference*, pages 229–233. ACM, 1966. 2

[29] Y.-W. Tai, H. Du, M. S. Brown, and S. Lin. Correction of spatially varying image and video motion blur using a hybrid camera. *IEEE Transactions on Pattern Analysis and Machine Intelligence*, 2009. 2

[30] R. N. Tubbs. *Lucky Exposures: Diffraction limited astronomical imaging through the atmosphere*. PhD thesis, Cambridge Univ., 2003. 5

[31] L. Yuan, J. Sun, L. Quan, and H.-Y. Shum. Image deblurring with blurred/noisy image pairs. *ACM Transactions on Graphics (SIGGRAPH)*, 2008. 2